RZ 3866 (#ZUR1311-002) 11/01/2013
Physical Sciences 11 pages

# Research Report

## A variable-temperature nanostencil compatible with a low-temperature STM/AFM

Wolfram Steurer, Leo Gross, Reto R. Schlittler, and Gerhard Meyer

IBM Research – Zurich
8803 Rüschlikon
Switzerland


The final version of this paper appeared in *Rev. Sci. Instrum.* **85**, 023706 (2014) and may be downloaded at http://dx.doi.org/10.1063/1.4864296

# A variable-temperature nanostencil compatible with a low-temperature STM/AFM

Wolfram Steurer,* Leo Gross, Reto R. Schlittler, and Gerhard Meyer

*IBM Research-Zurich, 8803 Rüschlikon, Switzerland*

## Abstract

We describe a nanostencil lithography tool capable of operating at variable temperatures down to 30 K. The setup is compatible with a combined low-temperature scanning tunneling microscope/ atomic force microscope (LT STM/AFM) located within the same ultra-high-vacuum apparatus. The lateral movement capability of the mask allows the patterning of complex structures. To demonstrate operational functionality of the tool and estimate temperature drift and blurring, we fabricated LiF and NaCl nanostructures on Cu(111) at 77 K.

PACS numbers: 68.37.Hk, 81.16.Rf, 81.16.Nd

Nanostencil lithography (NSL) is a resistless technique in which material is evaporated in ultra-high vacuum (UHV) through a stencil mask directly onto the substrate. Atomically clean, high-quality structures with lateral extensions down to a few tens of nanometers[1–3] and as thin as a few atomic layers[4] can be fabricated in this way. The stencil technique [5–15] can be applied to a broad range of substrates[16–21], and virtually any vacuum-evaporable material can be deposited[1–3,6,7,22–24]. Limitations of NSL are mainly imposed by geometrical constraints of the shadow mask and the limited lifetime of the mask due to clogging and mechanical stress. As an immediate consequence, patterns are limited to structures with simple topologies in the simple static mode. This limitation can be overcome in the dynamic[3,12,24] and the multistep[3,6,25] mode, allowing the fabrication of complex multi-material structures. However, in the dynamic mode, larger substrate-mask separations have to be chosen at the expense of lateral resolution. The gap between the mask and the substrate produces a blurring in the deposited structure, thus reducing the resolution of NSL. As analyzed by Vazquez-Mena *et al.* in detail[26], blurring is also affected by the properties of the deposited material and the substrate temperature during deposition. Long-range surface diffusion in particular is an issue for the fabrication of metal electrodes or for growth of adsorbate/substrate systems with small diffusion barriers. For example, Au clusters diffuse up to several 100 nm when evaporated onto a sample held at room temperature (RT)[27,28]. Therefore, operation at temperatures below RT during evaporation as well as imaging is a highly desirable goal. This is in particular true for STM-based single molecule manipulation experiments.

Here we describe a new variable-temperature NSL setup that is compatible with a combined LT STM/AFM located within the same UHV chamber. We demonstrate operational functionality of the new variable-temperature nanostencil by fabricating LiF and NaCl nanostructures on Cu(111) single-crystal surfaces at 77 K. Edge profile widths below 30 nm are achieved for structures that are 1.5 to 10 nm thick.

## I. NANOSTENCIL SETUP

A schematic view of the setup is shown in Fig. 1. It has three main parts: a multiple molecular beam epitaxy (MBE) source (home-built; with 4 metal electron-beam cells and 4 Knudsen cells), a standard *CreaTec*[29] sample holder attached to a liquid-He/liquid-$N_2$-

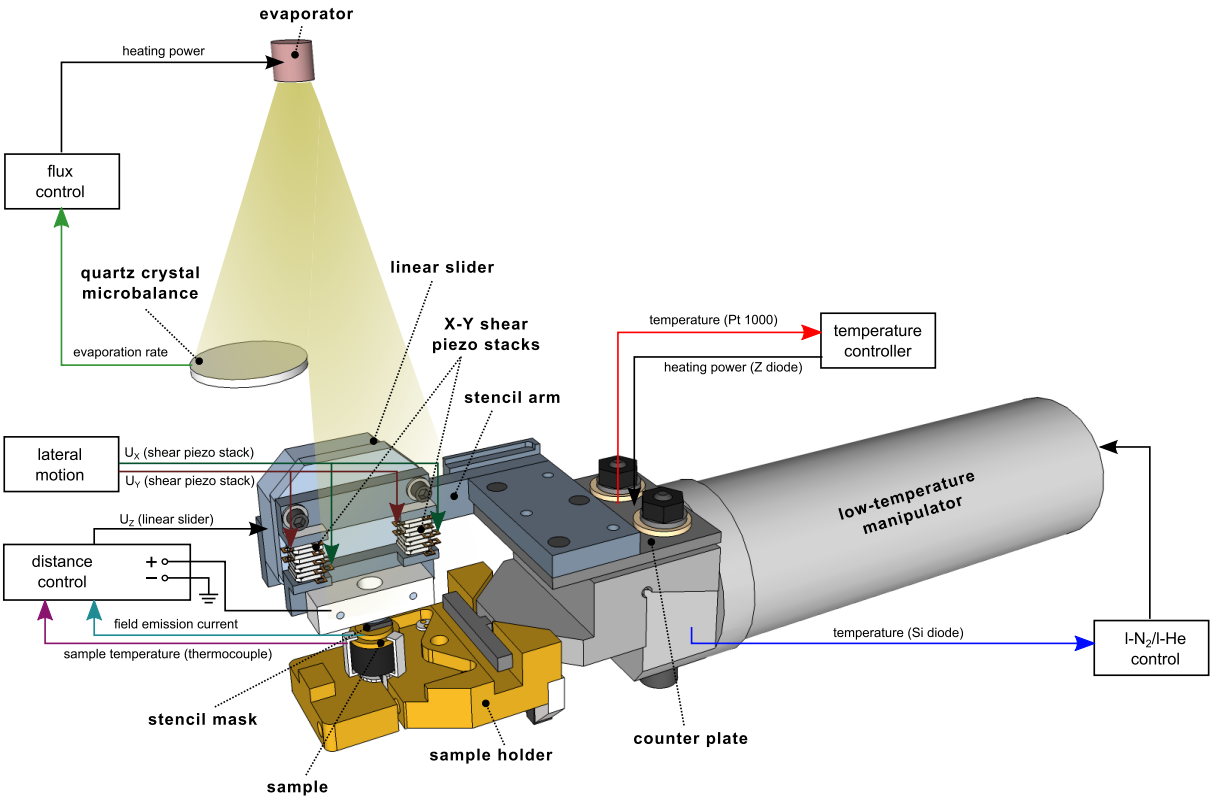


FIG. 1: Schematic view of the variable-temperature nanostencil setup. Also shown are the various control loops active during stenciling.

cooled LT manipulator, and the stencil device consisting of a mask, a linear slider stage (*AttoCube*[30] ANPx101/LT/UHV with 5 mm $Z$-movement range) and shear piezo stacks for $X$-$Y$ lateral motion capability (*Noliac*[31] CSAP02 shear plate actuators, 4 shear actuators per stack, 4×1.5 $\mu$m free stroke from –320 to 320 V). The mask sits on the slider stage, which is connected to the LT manipulator via the stencil arm. The complete stencil part is removable and can be put into a storage position or transferred into a load lock. On the LT manipulator side, the stencil part is held by magnets and aligned with pins embedded into a counter plate at the LT manipulator head. PEEK (polyether ether ketone) spacers are used to insulate the counter plate electrically and thermally from the LT manipulator. Heating elements (2 Zener-diodes in series; maximum heating power of 4 W) and a Pt1000 temperature sensor glued to the counter plate serve to control the temperature of the stencil part. The distance between the sample and the evaporator source is 250 mm in our UHV

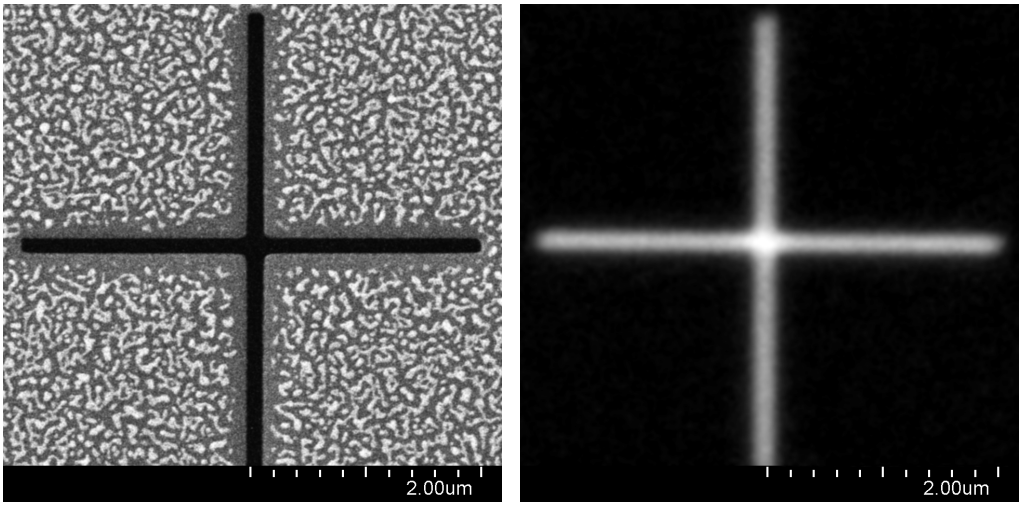


(a) (b)

FIG. 2: SEM images of (a) stencil mask and (b) 10-nm-thick LiF structure fabricated on Cu(111).

apparatus.

In the NSL tool, the stencil mask is moved towards the substrate surface using the linear slider stage and laterally using the $X$-$Y$ piezo stacks. The mask is aligned parallel with the substrate using a rotatable mask holder[3] that self-aligns upon gently pressing the mask against the substrate surface. After alignment, the mask is retracted a couple of nanometers and the mask-sample distance is monitored via the field-emitted current induced by a $\pm 15$ V ramp applied to the mask. The substrate (silicon wafer, metal single crystals) is mounted on a standard *CreaTec* sample holder with an integrated resistive heater and cooled via the LT manipulator. The substrate temperature is monitored using a thermocouple.

## II. EXPERIMENT

For the experiments shown here, we have used a Cu(111) crystal as the substrate material. Prior to stenciling, we thoroughly cleaned the crystal surface by cycles of extended $Ne^+$ sputtering (1 kV, 20 $\mu$A/cm$^2$) and short annealing periods at 900 K. To avoid damage to the stencil masks the smoothness and cleanliness of the crystal surface were checked at regular intervals in an external scanning electron microscope (SEM). The cleaning procedure was continued until no contaminations of particles could be detected anymore.

Stencil masks were fabricated by structuring silicon-nitride membranes with a focused ion beam (FIB) (FEI Helios 450S). The 150-nm-thick silicon nitride membranes with an

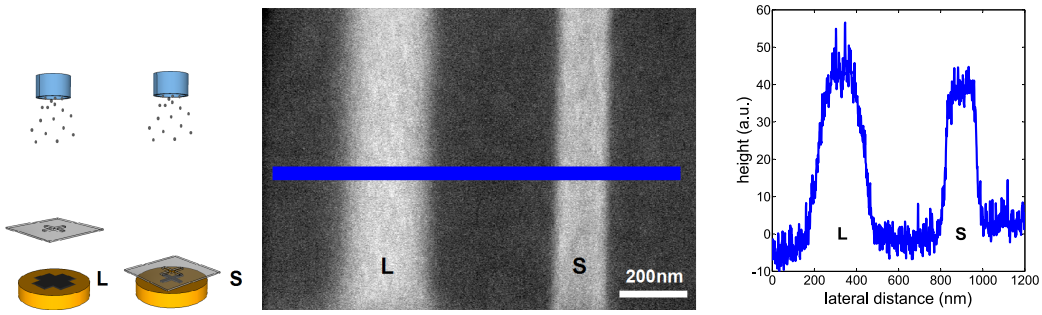


(a) (b) (c)

FIG. 3: 10-nm-thick LiF structures evaporated on Cu(111) at large (L) and small (S) mask-substrate separation, respectively, using the mask shown in Fig. 2a. (a) Schematic views, (b) SEM image showing a segment of the vertical beam of the cross, and (c) height profile taken at the position indicated by the blue line in (b).

area of 500 $\mu$m$^2$ were etched into silicon carrier chips (membranes from *Aquamarijn*[32]) and were coated with 30-nm-thick conducting Au film on both sides prior to FIB treatment. Alternatively, we used perforated carbon films purchased from *Quantifoil*[33]. LiF and NaCl was evaporated at a rate of 3 nm/min using a thermal effusion cell.

Figure 2a shows an SEM image of the $Si_3N_4$ mask used before stenciling. The cross structure consists of two identical apertures that are 4 $\mu$m long and 150 nm wide. The contrast on the $Si_3N_4$ membrane is due to the formation of gold islands. A 10-nm LiF structure evaporated through this mask onto Cu(111) at 77 K and as imaged at RT in an external SEM is shown in Fig. 2b. In this image, the Cu(111) substrate appears dark and the LiF structure bright.

Two subsequently performed evaporations of 5-nm LiF onto Cu(111) at 77 K, reusing the mask displayed in Fig. 2a at a large and a small mask-substrate separation, are shown in Fig. 3. A schematic representation of the two situations is displayed in panel (a). Panel (b) shows an SEM image of the stenciled segment of the vertical beam of the cross structure (see Fig. 2a). Again, the Cu(111) surface appears dark and the LiF structures bright. A height profile taken at the position indicated by the blue line (b) is displayed in (c). For the structure on the right, an edge profile width <30 nm (10–90%) is found.

Figure 4 depicts SEM images of the perforated carbon mask before stenciling. The supporting copper grid, 300 mesh, appears bright in the SEM image, see Fig. 4a. The

carbon film is covered with identical holes that are 1.2 $\mu$m in diameter (5 $\mu$m center-to-center distance); a closeup of a single hole is shown in Fig. 4b. Figure 4c displays a 1.5 nm NaCl structure evaporated through this mask onto Cu(111) at 77 K and imaged at 5 K in the LT STM/AFM located in the same UHV apparatus. To enhance the cristallinity of the evaporated NaCl structure, the sample was annealed at 250 K for 1 min immediately after deposition. The collage of STM images[34] in (c) reveals a series of Cu step bunches below the stenciled NaCl structure. The NaCl film appears as a broken-up structure composed of arbitrarily oriented NaCl crystallites (bright) with patches of the Cu surface in between (dark). This kind of surface morphology is expected for annealed NaCl on Cu(111) because the fourfold NaCl film grows incommensurately on the 3-fold Cu(111) substrate surface. The edge of the structure appears sharp, with no notable change of the size distribution of the crystallites in the border region.

## III. DISCUSSION

For the field of application envisage, namely the combination of the stenciling technique with single-molecule-manipulation experiments, utmost cleanliness and well-defined borders of the stenciled structures are the two major requirements. The former puts very high demand on the cleanliness of the mask and the stenciling process itself. To keep contaminations by residual gases low, evaporation of the structures should take place as quickly as possible after the last cleaning cycle of the substrate. Likewise, the time span between stenciling and the transfer to the LT STM/AFM should be short. For this purpose, the stencil device can quickly be transferred to and from the manipulator. Once the stencil device has been removed, fabricated structures can be transferred directly into the LT STM/AFM within less than 5 min.

To achieve well-defined borders, full control over the substrate temperature is required in general. On the one hand, surface diffusion can lead to a significant broadening of stenciled structures, which can be suppressed by lowering the substrate temperature during evaporation. On the other hand, if crystalline growth is desired, post-annealing of the evaporated structures can become necessary. This is especially the case if the deposition takes place at low substrate temperatures. As the stencil is constructed on a standard *CreaTec* UHV liquid-He-cooled manipulator, the substrate temperature can be varied from

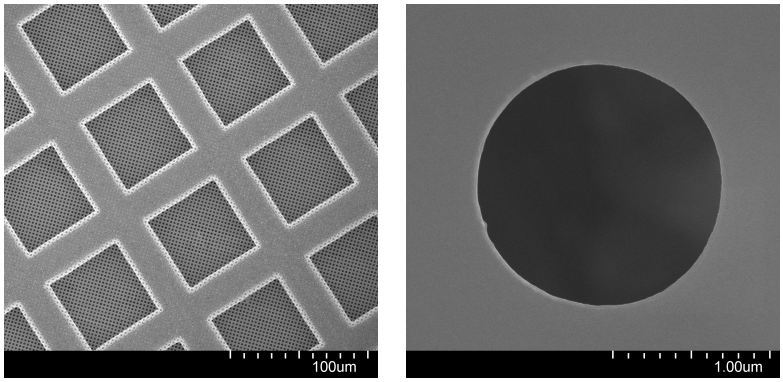


(a) (b)

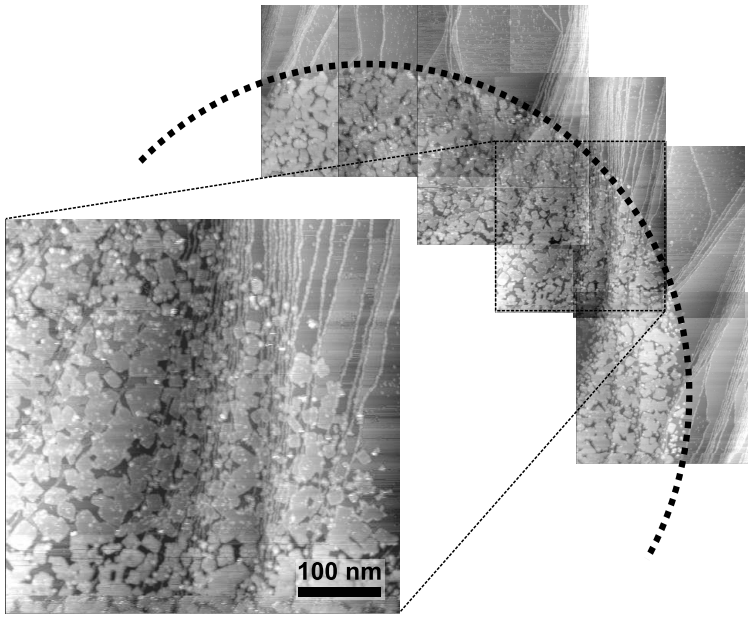


(c)

FIG. 4: SEM images of a carbon mask with evenly distributed 1.2-$\mu$m holes [(a) - overview, (b) closeup of a single hole]. (c) Collage of STM images of a 1.5 nm NaCl structure evaporated onto Cu(111) through this mask. Imaging details: 480×480 nm$^2$, U = 5.0 V, I = 0.8 pA (all images).

30 K to 800 K or even higher, as specified by the manufacturer.

Before and after stenciling, the stencil device is placed in a storage position within the UHV chamber or on a transfer rod so that it can be transferred out of the UHV chamber via a load lock. This ease of exchangeability makes it possible to fabricate multilayer structures. For this reason, stencil masks are prealigned on the mask holder using an optical microscope prior to mounting them on the stencil arm and inserting them into the UHV tool.

To minimize thermal drift of the mask with respect to the substrate, the stencil part is

kept at RT at all times. This is necessary because the time response of the stencil part to a temperature change is very slow: Reaching a sufficiently stable thermal equilibrium takes several hours, too long to keep the sample surface clean. Thermal drift is caused by thermal expansion, which is proportional to the thermal expansion coefficient, the length, and the temperature change. As the stencil part is relatively long ($\approx$ 100 mm), even a tiny temperature variation of 0.01 K during evaporation would distort the fabricated structure by several tens of nanometers. For this reason, the temperature of the counter plate, which holds the stencil part, is kept at RT by a PID controller.

The rather large temperature difference between the substrate and the mask entails other challenges. Most notably, in the present design, mechanical contact between substrate and mask should be avoided. At the same time, however, one wishes to keep the mask-substrate distance as small as possible to reduce the geometrical blurring of the structures fabricated. Moreover, it is highly desirable to have feedback information about the mask-substrate distance and the temporal stability of their relative positions, especially during evaporation. We overcome this problem by using very small mask-substrate separations of only a couple of nanometers. At this distance, field-electron emission can be observed even for low bias voltages (typically $\pm$15 V). By constantly measuring the field-electron emission behavior as a function of the applied bias voltage (measuring the so-called Fowler-Nordheim $I$-$V$ curves) the temporal stability of the mask position with respect to the substrate can be monitored.

The dependence of the broadening on the mask-substrate separation is demonstrated in Fig. 3b. The spread of the 10-nm-thick LiF structure at large mask-substrate separation (see Fig. 3b, left structure) fits well with the expected broadening at the gap value of $30 \pm 5$ $\mu$m chosen. At close mask-substrate separation, the edge profile width is below 30 nm. However, as the contrast variation in SEM does not necessarily correspond to the real structure height, we refrain from presenting a detailed analysis of the broadening based on SEM images.

The 1.5-nm-thick NaCl structure, imaged at 5 K in the LT STM/AFM and shown in Fig. 4, does not exhibit a significantly sharper border region than the LiF structure. However, the LT STM image reveals that the border region is well-defined in the sense that the transition from the NaCl structure to the Cu substrate is abrupt; no additional broadening of the stenciled structure due to surface diffusion is apparent. This is an important observation and a piece of information that SEM cannot provide. It is of particular interest as the NaCl structure was tempered at 250 K after evaporation.

In contrast to SEM, LT STM/AFM is sensitive to single molecules and can provide information about the cleanliness of the fabricated structure at a molecular level. Reaching the high degree of cleanliness required for combining the stencil technology with single molecule manipulation is an aspect we still have to work on. The LT STM image shown in Fig. 4c reveals contaminations by small organic molecules that presumably were transferred from the mask to the substrate during the alignment procedure. On the NaCl structure, the polluting molecules appear as white speckles, whereas on the Cu substrate they preferentially decorate the step edges. We think that the contamination problem is caused primarily by the epoxy glue we used to attach the perforated carbon mask to the mask holder.

## IV. CONCLUSIONS

We have presented a new variable-temperature nanostencil tool that is compatible with an LT STM/AFM system. The setup offers full temperature control during structure fabrication, sample transfer, and imaging. This makes it a promising tool for growing high-quality epitaxial structures and opens up a door for using artificial nano-structures in low-temperature STM/AFM experiments.

### Acknowledgements

We thank R. Allenspach for helpful comments and acknowledge financial support by the EU project 'ARTIST' (Contract No. 243421), the ERC Advanced Grant 'CEMAS' and the Swiss NCCR 'Nanoscale Science'.

### References

* Electronic address: wst@zurich.ibm.com

[1] M. M. Deshmukh, D. C. Ralph, M. Thomas, and J. Silcox, Applied Physics Letters **75**, 1631 (1999).

[2] A. R. Champagne, A. J. Couture, F. Kuemmeth, and D. C. Ralph, Applied Physics Letters **82**, 1111 (2003).

[3] P. Zahl, M. Bammerlin, G. Meyer, and R. R. Schlittler, Review of Scientific Instruments **76**, 023707 (2005).

[4] R. Allenspach, A. Bischof, M. Stampanoni, D. Kerkmann, and D. Pescia, Applied Physics Letters **60**, 1908 (1992).

[5] K. Ono, H. Shimada, S.-i. Kobayashi, and Y. Ootuka, Japanese Journal of Applied Physics **35**, 2369 (1996).

[6] J. Lee, B. Ju, J. Jang, Y. Yoon, and J. Kim, Journal of Materials Science **42**, 1026 (2007).

[7] K. Sidler, N. V. Cvetkovic, V. Savu, D. Tsamados, A. M. Ionescu, and J. Brugger, Sensors and Actuators A: Physical **162**, 155 (2010).

[8] J. A. Merlo and C. D. Frisbie, The Journal of Physical Chemistry **108**, 19169 (2004).

[9] T. Uchihashi, U. Ramsperger, T. Nakayama, and M. Aono, Japanese Journal of Applied Physics **47**, 1797 (2008).

[10] L. Gross, R. R. Schlittler, G. Meyer, L. A. Fendt, F. Diederich, T. Glatzel, S. Kawai, S. Koch, and E. Meyer, Journal of Vacuum Science & Technology B: Microelectronics and Nanometer Structures **28**, C4D34 (2010).

[11] V. Savu, S. Neuser, G. Villanueva, O. Vazquez-Mena, K. Sidler, and J. Brugger, Journal of Vacuum Science & Technology B: Microelectronics and Nanometer Structures **28**, 169 (2010).

[12] L. Gross, R. R. Schlittler, G. Meyer, A. Vanhaverbeke, and R. Allenspach, Applied Physics Letters **90**, 093121 (2007).

[13] L. Gross, R. R. Schlittler, G. Meyer, and R. Allenspach, Nanotechnology **21**, 325301 (2010),

[14] O. Vazquez-Mena, G. Villanueva, V. Savu, K. Sidler, M. A. F. van den Boogaart, and J. Brugger, Nano Letters **8**, 3675 (2008).

[15] C. Joachim, D. Martrou, M. Rezeq, C. Troadec, D. Jie, N. Chandrasekhar, and S. Gauthier, Journal of Physics: Condensed Matter **22**, 084025 (2010).

[16] E. Speets, P. te Riele, M. van den Boogaart, L. Doeswijk, B. Ravoo, G. Rijnders, J. Brugger, D. Reinhoudt, and D. Blank, Advanced Functional Materials **16**, 1337 (2006).

[17] Y. X. Zhou, A. T. Johnson, J. Hone, and W. F. Smith, Nano Letters **3**, 1371 (2003).

[18] K. Sidler, O. Vazquez-Mena, V. Savu, G. Villanueva, M. van den Boogaart, and J. Brugger, Microelectronic Engineering **85**, 1108 (2008).

[19] G. Villanueva, O. Vazquez-Mena, M. van den Boogaart, K. Sidler, K. Pataky, V. Savu, and J. Brugger, Microelectronic Engineering **85**, 1010 (2008).

[20] S. W. Pang, M. W. Geis, W. D. Goodhue, N. N. Efremow, D. J. Ehrlich, R. B. Goodman, and J. N. Randall, Journal of Vacuum Science & Technology B: Microelectronics and Nanometer Structures **6**, 249 (1988).

[21] B. Grévin, M. Fakir, J. Hayton, M. Brun, R. Demadrille, and J. Faure-Vincent, Review of Scientific Instruments **82**, 063706 (2011).

[22] J. Brugger, J. Berenschot, S. Kuiper, W. Nijdam, B. Otter, and M. Elwenspoek, Microelectronic engineering **53**, 403 (2000).

[23] C.-V. Cojocaru, C. Harnagea, F. Rosei, A. Pignolet, M. A. F. van den Boogaart, and J. Brugger, Applied Physics Letters **86**, 183107 (2005).

[24] S. Egger, A. Ilie, Y. Fu, J. Chongsathien, D. Kang, and M. E. Welland, Nano Letters **5**, 15 (2004).

[25] S. Egger, S. Higuchi, and T. Nakayama, Journal of Combinational Chemistry **8**, 275 (2006).

[26] O. Vazquez-Mena, L. G. Villanueva, V. Savu, K. Sidler, P. Langlet, and J. Brugger, Nanotechnology **20**, 415303 (2009).

[27] T. Tun, M. Lwin, H. Kim, N. Chandrasekhar, and C. Joachim, Nanotechnology **18**, 335301 (2007).

[28] A. Linklater and J. Nogami, Nanotechnology **19**, 285302 (2008).

[29] SPS-CreaTec GmbH, Magnusstr. 11, 12489 Berlin, Germany

[30] Attocube systems AG, Königinstrasse 11a, 80539 München, Germany

[31] Noliac A/S, Hejreskovvej 18,3490 Kvistgaard, Denmark

[32] Aquamarijn Micro Filtration BV, Berkelkade 11, NL 7201 JE Zutphen, The Netherlands

[33] Quantifoil Micro Tools GmbH, In den Brückenäckern 4, 07751 Großlöbichau, Germany

[34] At 5 K, the scan range of the scanner is approximately 500 nm, significantly less than the extension of the evaporated structure.